Anomalous relaxation of coarsening foams with viscoelastic continuous phase.

Supplementary Information

Chiara Guidolin,[a,*] Emmanuelle Rio,[b] Roberto Cerbino,[c] Anniina Salonen,[b] and Fabio Giavazzi[a,*]

[a] *Department of Medical Biotechnology and Translational Medicine, University of Milan, Segrate, Italy.*

[b] *Université Paris-Saclay, CNRS, Laboratoire de Physique des Solides, Orsay, France.*

[c] *Faculty of Physics, University of Vienna, Vienna, Austria.*

* chiara.guidolin@unimi.it, fabio.giavazzi@unimi.it

1 Extended DDM results

The image structure function $d(q, \Delta t)$ obtained from DDM analysis is first fitted with a function of the kind $d(q, \Delta t) = A(q)[1 - f(q, \Delta t)] + B(q)$, where $f(q, \Delta t)$ is a compressed exponential function $f(q, \Delta t) = \exp[-(\Gamma(q)\Delta t)^{\alpha(q)}]$ and the compressing exponent $\alpha(q)$ is left as a free parameter to check its dependence on q. The compressing exponent $\alpha(q)$ is shown in Fig. S1 for each ϕ at each foam age t^*, where we can see that it displays only a weak q-dependence. We thus evaluate the average compressing exponent $\alpha = \langle \alpha(q) \rangle$ by averaging over a range of q for which at least the first 10% of the decay of $f(q, \Delta t)$ is visible and the amplitude is larger than the noise.

We then fit the same data again with a compressed exponential where the compressing exponent is fixed to be equal to its mean value. Results obtained from this fit are reported in Fig. S2, S3, and S4 for each sample at foam age $t^* = 1800$, 2700, and 3600 seconds respectively. Each figure contains representative examples of intermediate scattering functions $f(q, \Delta t)$ computed at different wavevectors q, the amplitude $A(q)$ and the noise term $B(q)$, as well as the relaxation rate $\Gamma(q)$. The vertical dashed line in the graphs of $\Gamma(q)$ represents the wavevector corresponding to the a length scale of the order of the typical bubble size R^*, namely $q^* = 2\pi/R^*$. Each column refers to a different oil fraction ϕ (65%, 70%, 75%, and 80% from left to right). The selected range of wavevectors q is highlighted with coloured symbols.

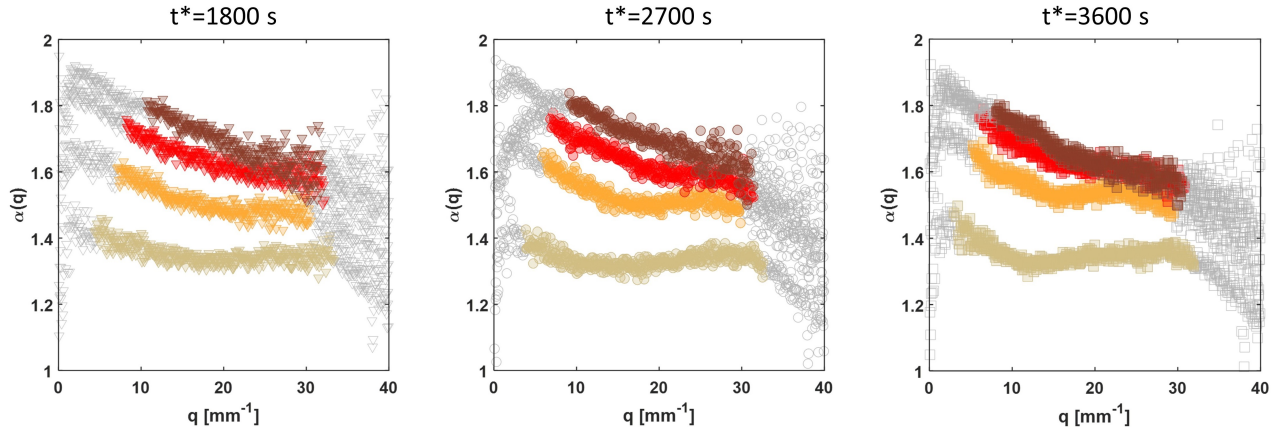

Figure S1: Compressing exponent $\alpha(q)$ obtained from a first fit of the image structure functions.

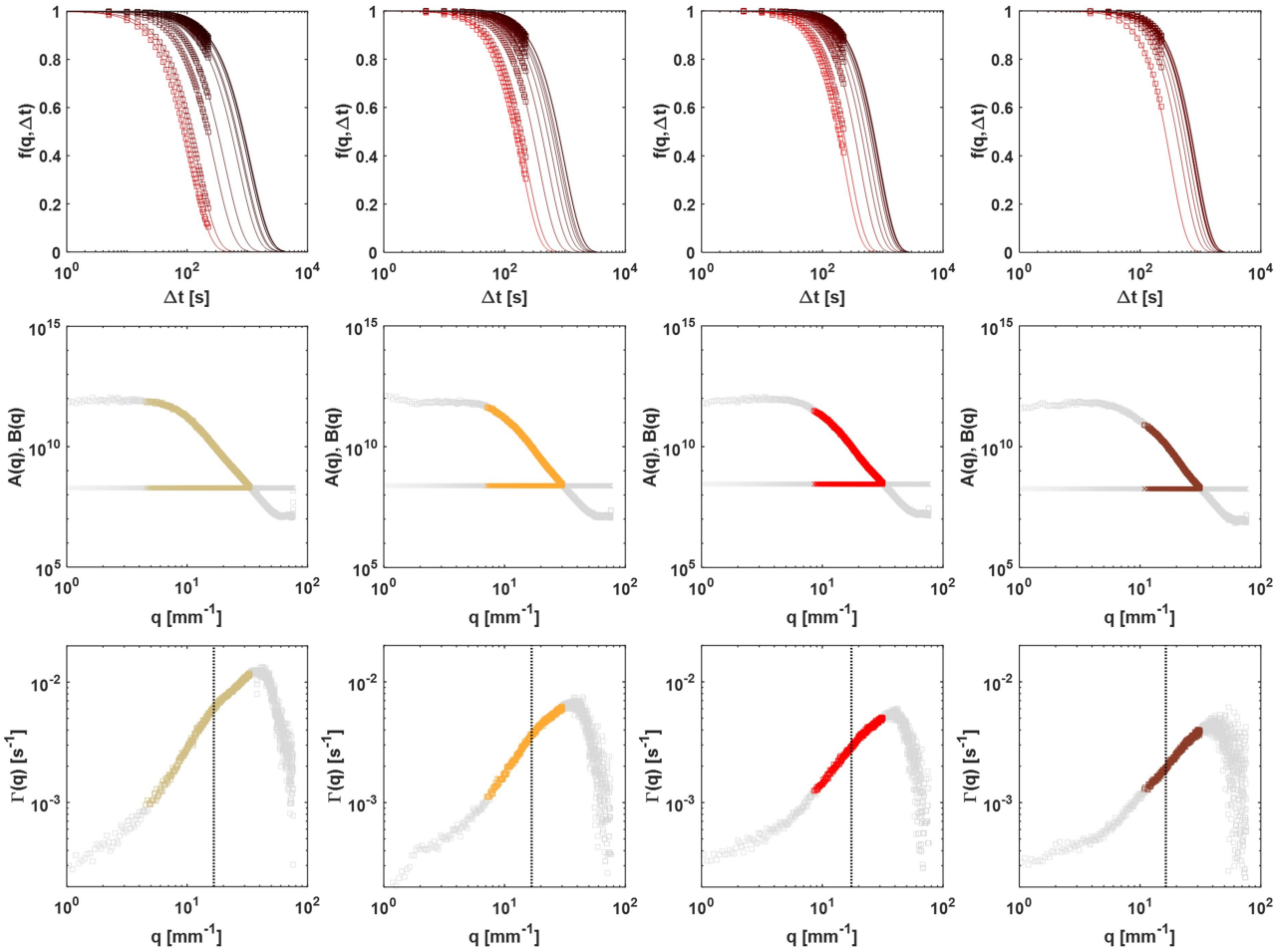

Figure S2: Fit results for the time window centered at $t^* = 1800$ s. Each column correspond to a different oil fraction ϕ (65%, 70%, 75%, and 80% from left to right). First row: representative examples of intermediate scattering function $f(q, \Delta t)$ for different wavevectors q. Empty squares represent experimental data. The solid lines represent a compressed exponential fit to the data with fixed compressing exponent α. Second row: amplitude $A(q)$ and noise term $B(q)$ obtained from the fit over the whole range of accessible q. Coloured symbols highlight the selected range of q. Third row: relaxation rate $\Gamma(q)$. The vertical dashed line marks the wavevector $q^* = 2\pi/R^*$.

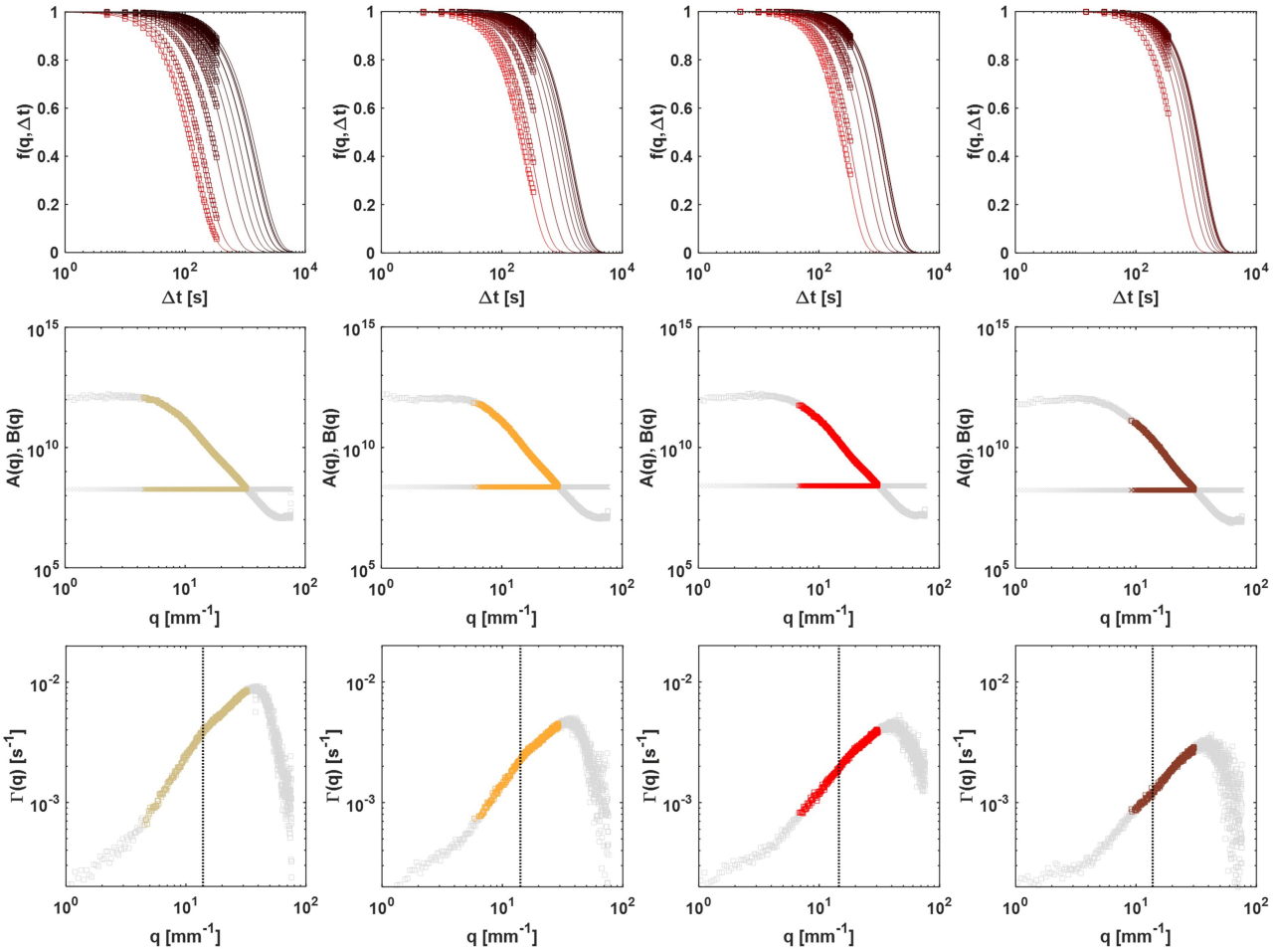

Figure S3: Fit results for the time window centered at $t^* = 2700$ s. Each column correspond to a different oil fraction ϕ (65%, 70%, 75%, and 80% from left to right). First row: representative examples of intermediate scattering function $f(q, \Delta t)$ for different wavevectors q. Empty squares represent experimental data. The solid lines represent a compressed exponential fit to the data with fixed compressing exponent α. Second row: amplitude $A(q)$ and noise term $B(q)$ obtained from the fit over the whole range of accessible q. Coloured symbols highlight the selected range of q. Third row: relaxation rate $\Gamma(q)$. The vertical dashed line marks the wavevector $q^* = 2\pi/R^*$.

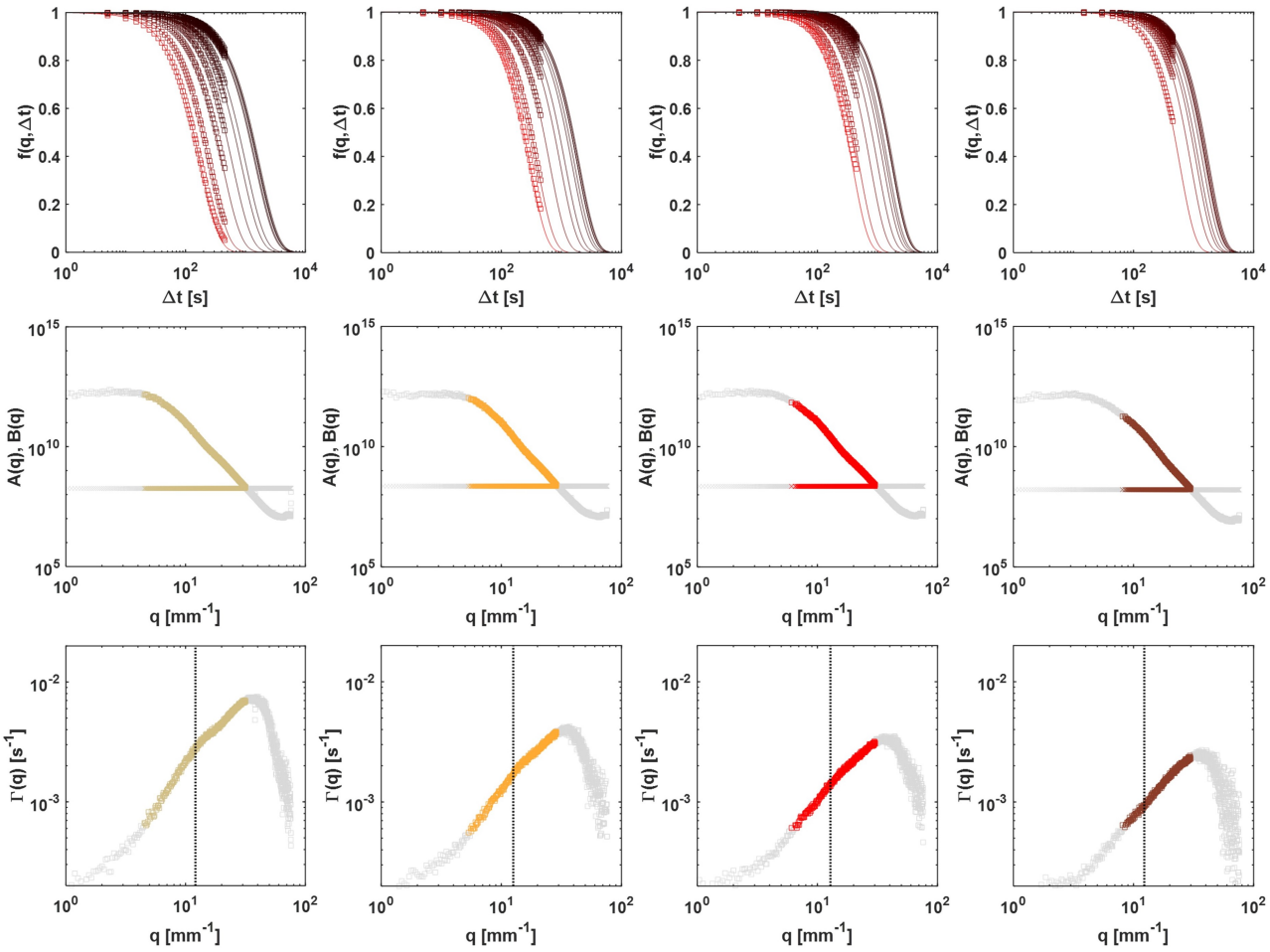

Figure S4: Fit results for the time window centered at $t^* = 3600$ s. Each column correspond to a different oil fraction ϕ (65%, 70%, 75%, and 80% from left to right). First row: representative examples of intermediate scattering function $f(q, \Delta t)$ for different wavevectors q. Empty squares represent experimental data. The solid lines represent a compressed exponential fit to the data with fixed compressing exponent α. Second row: amplitude $A(q)$ and noise term $B(q)$ obtained from the fit over the whole range of accessible q. Coloured symbols highlight the selected range of q. Third row: relaxation rate $\Gamma(q)$. The vertical dashed line marks the wavevector $q^* = 2\pi/R^*$.

2 Displacement correlations

We investigate how single-bubble motility depends on the bubble size. To account for the different average motility of different samples, we consider for each sample a different time delay Δt, corresponding to the same global mean square displacement (MSD), as shown in Fig. S5 (a). Thus, we calculate the MSD for each single bubble and plot it against the bubble radius R. Results are shown in Fig. S5(b) for all oil fractions ϕ. Only a mild dependency on the bubble size is observed, not compatible with the scaling $MSD \propto R^{-1}$ recently reported for a dense ripening emulsion [1].

For the same time delays, we also compute the spatial correlation function of bubble displacements as $\langle \delta \mathbf{r}_m \cdot \delta \mathbf{r}_n \rangle(r) / \langle \delta r^2 \rangle$, where n and m label distinct bubbles at a distance r, while $\delta \mathbf{r}_n$ and $\delta \mathbf{r}_m$ are the respective displacements. Results are compared in Fig. S5(c), where we can see that the correlation functions do not change significantly with ϕ, revealing that the correlation properties of the displacement field are similar between all samples.

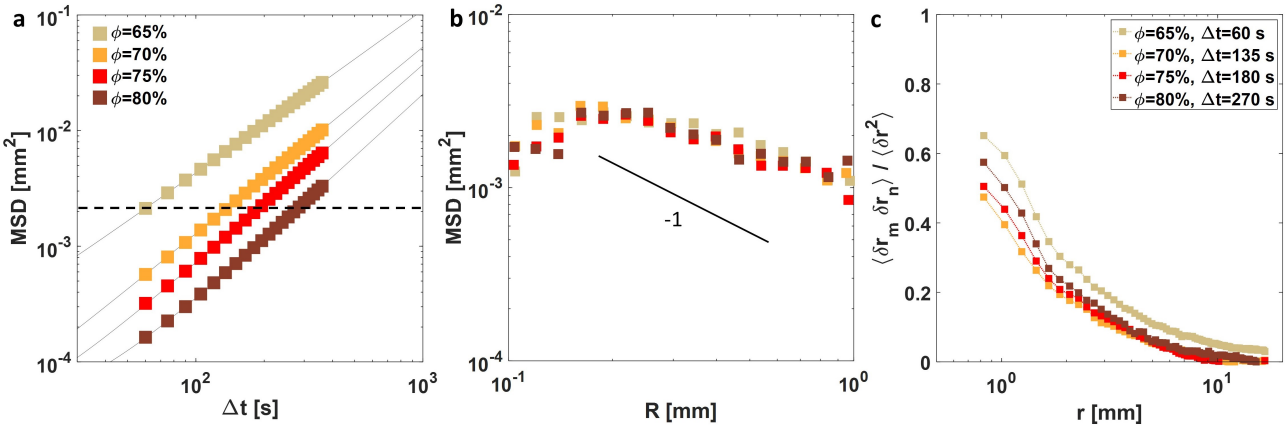

Figure S5: **Displacement correlations.** (a) Δt-dependence of the global MSD at different ϕ (from [2]). (b) Dependency of the single-bubble MSD on the bubble radius. The samples are compared at different time delays corresponding to the same global MSD, as indicated by the horizontal dashed line in (a). (c) Displacement correlation for the different samples evaluated at time delays corresponding to the same MSD.

3 Distributions of bubble displacements

For each foam sample, we calculated the distribution of bubble displacements Δr for increasing time delays Δt (from 60 to $t^*/10$ seconds with a step of 15 seconds) at foam age $t^* = 1800$, 2700, and 3600 seconds, as reported in figures S6, S7, and S8 respectively.

For each ϕ and t^*, the probability distribution of bubble displacements systematically shifts to larger displacements with increasing time delays Δt [2]. The position of the distribution peak grows linearly over time: a simple normalization with the lag time Δt indeed leads to an excellent data collapse, consistent with ballistic-like bubble motion at short length scales.

This normalization highlights a power-law decay $P(\Delta r, \Delta t)\Delta t \sim (\Delta r/\Delta t)^{-(\gamma+1)}$, with exponent γ increasing with ϕ, at bubble displacements right above the maximum peak, before sharply dropping at displacements of the order of the typical bubble size.

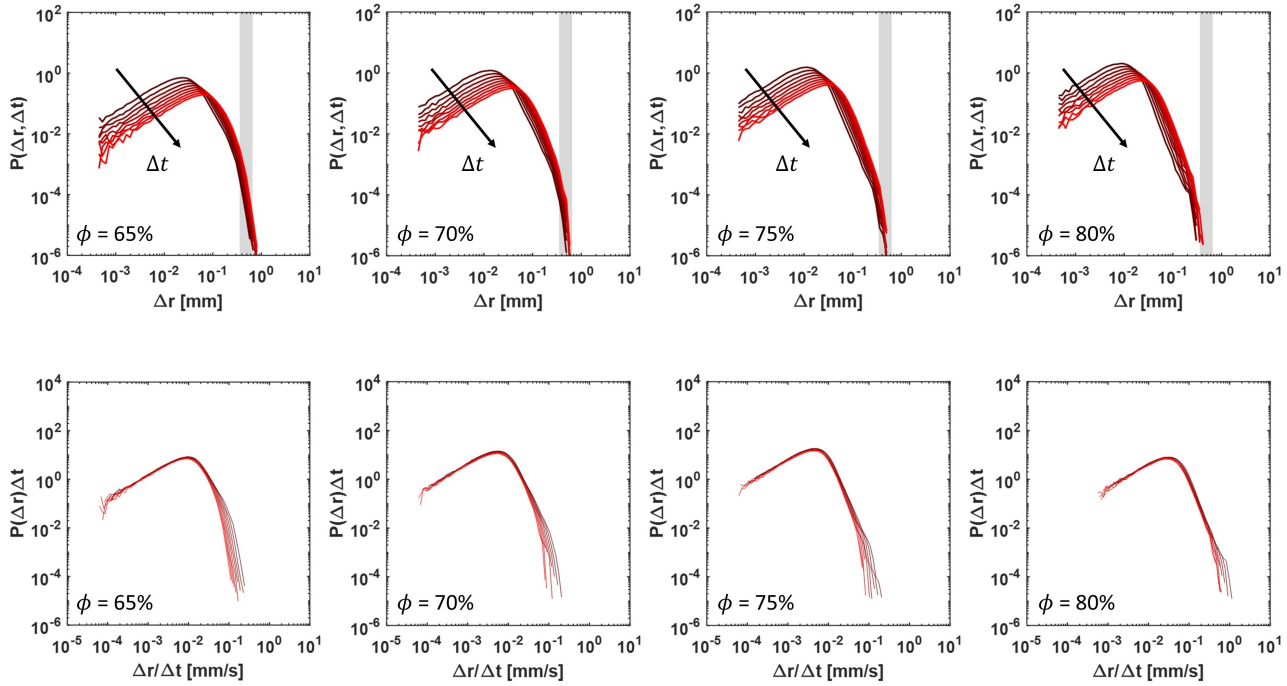

Figure S6: Distributions of bubble displacements for the time window centered around $t^* = 1800$ s. Top row: probability distribution of bubble displacements Δr at different time delays Δt. The vertical gray bar represents the typical bubble size. Bottom row: same distributions after normalisation with the time delay.

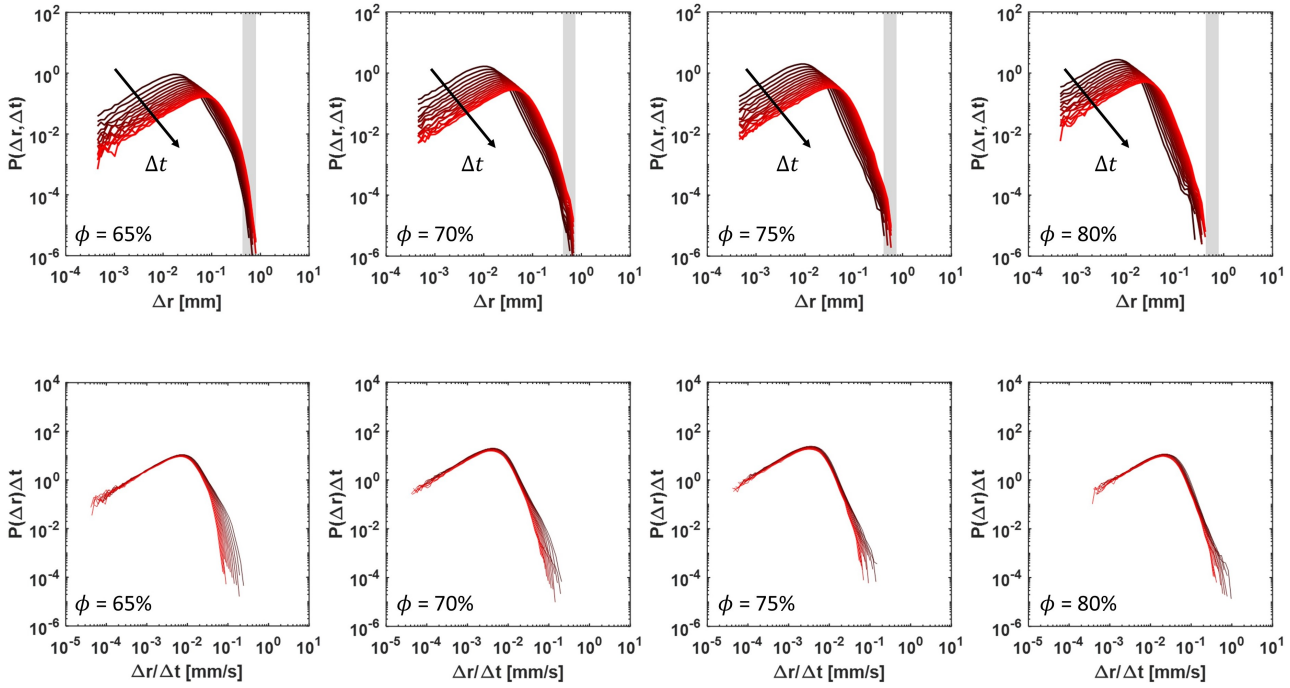

Figure S7: Distributions of bubble displacements for the time window centered around $t^* = 2700$ s. Top row: probability distribution of bubble displacements Δr at different time delays Δt. The vertical gray bar represents the typical bubble size. Bottom row: same distributions after normalisation with the time delay.

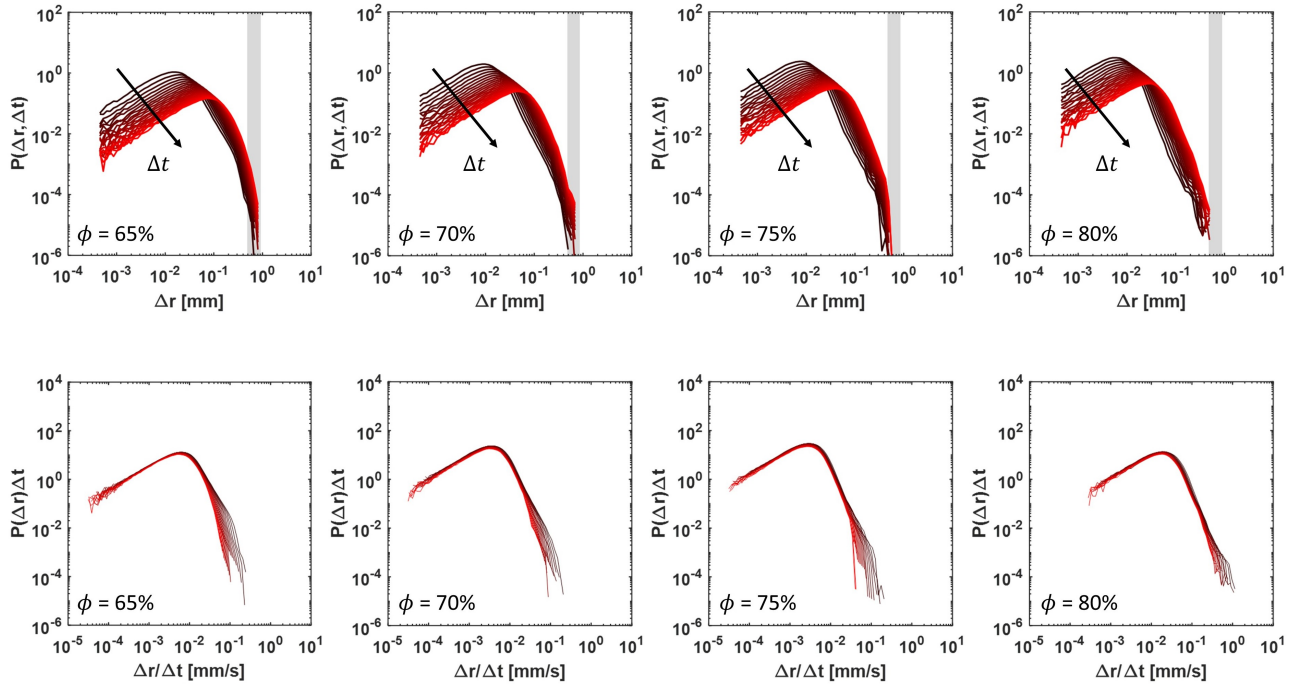

Figure S8: Distributions of bubble displacements for the time window centered around $t^* = 3600$ s. Top row: probability distribution of bubble displacements Δr at different time delays Δt. The vertical gray bar represents the typical bubble size. Bottom row: same distributions after normalisation with the time delay.

4 Apparently steeper power-law decay of pdf(Δr) for large compressing exponents

As discussed in the main text, if the intermediate scattering function is a compressed exponential of the kind $f(q, \Delta t) = \exp(-(v_0 q \Delta t)^\alpha)$, the probability distribution of particle displacements pdf(Δr) is expected to have a power-law tail decaying as $\sim -(1+\gamma)$ with $\gamma = \alpha$.

However, in foams at ϕ larger than 65% we observe a steeper power-law decay of pdf(Δr), with $\gamma > \alpha$. This can be ascribed to the finite size of the sample [3] which, at large compressing exponents, results in an initially steeper decay of the probability distribution of displacements.

In Fig. S9 we report the pdf(Δr) calculated for compressing exponents α between 1 and 1.9. We call γ_a the apparent exponent measured immediately after the maximum peak. We can see that, when α is only slightly larger than 1, we immediately recover the right scaling with $\gamma_a \simeq \alpha_t$. For the sample $\phi = 65\%$, indeed, we experimentally observe the right exponent, $\gamma = \alpha$. However, when α is larger than 1.5, the distributions exhibit a steeper decay with exponent $-(1+\gamma_a)$, with $\gamma_a > \alpha$, before reaching the right scaling. This explains why in our samples at higher ϕ we observe a power law tail steeper than expected. We stress that in our case we could not reach the right scaling as the bubble displacements are restricted to length scales smaller than the typical bubble size.

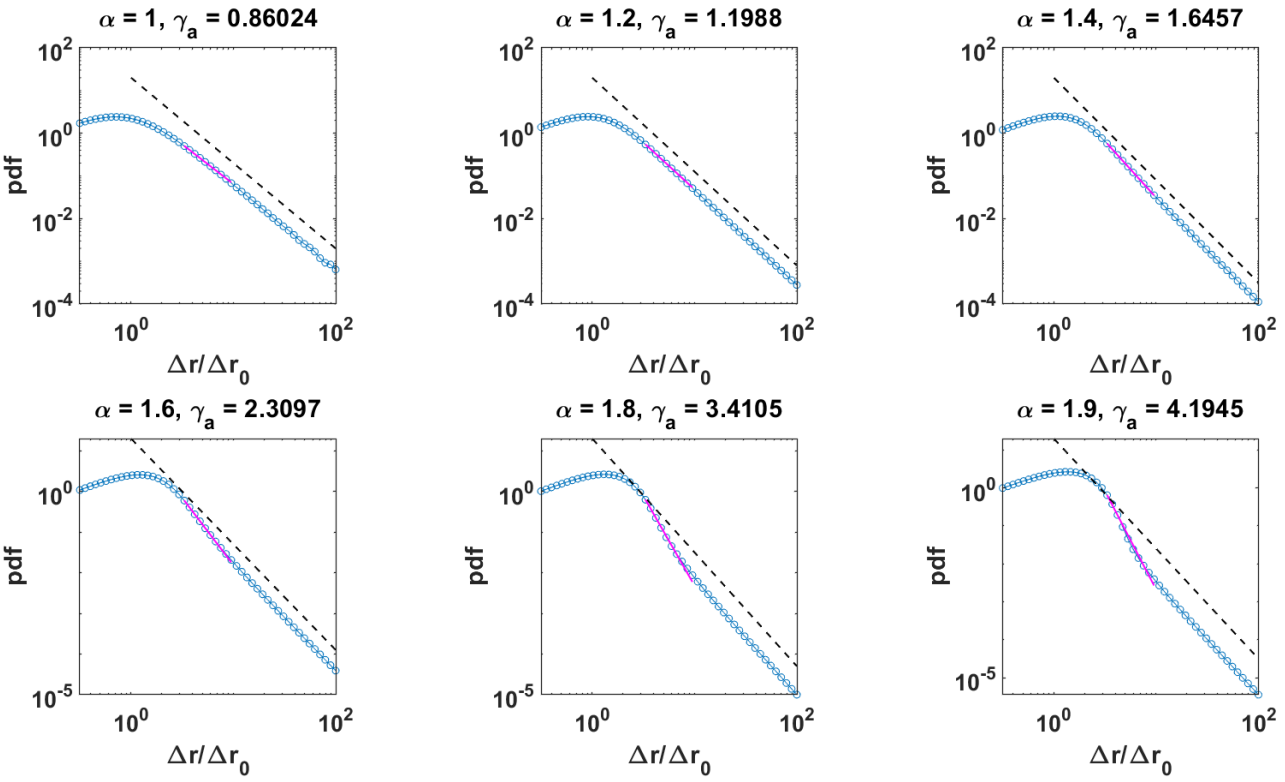

Figure S9: The graphs show the pdf of displacements expected for compressed exponential ISF having a compressing exponent α_t. The dashed line marks the expected power-law decay $\sim -(1+\gamma)$ with $\gamma = \alpha$. The apparent steeper decay with exponent $-(1+\gamma_a)$ with $\gamma_a > \alpha$, obtained from a power law fit, is indicated by the magenta solid line.

References

[1] Clary Rodríguez-Cruz, Mehdi Molaei, Amruthesh Thirumalaiswamy, Klebert Feitosa, Vinothan N Manoharan, Shankar Sivarajan, Daniel H Reich, Robert A Riggleman, and John C Crocker. Experimental observations of fractal landscape dynamics in a dense emulsion. Soft Matter, 19(35):6805–6813, 2023.

[2] Chiara Guidolin, Emmanuelle Rio, Roberto Cerbino, Fabio Giavazzi, and Anniina Salonen. Matrix viscoelasticity decouples bubble growth and dynamics in coarsening foams. arXiv:2405.09382 [cond-mat.soft], 2024.

[3] Rafał Weron. Levy-stable distributions revisited: tail index¿ 2 does not exclude the levy-stable regime. International Journal of Modern Physics C, 12(02):209–223, 2001.